Chemical Engineering Journal 102 (2004) 119–130

Chemical Engineering Journal

www.elsevier.com/locate/cej

Performance of a Co-Ni catalyst for propane reforming under low steam-to-carbon ratios

Kelfin M. Hardiman [a], Tan T. Ying [a], Adesoji A. Adesina [a,*], Eric M. Kennedy [b], Bogdan Z. Dlugogorski [b]

[a] *Reactor Engineering and Technology Group, School of Chemical Engineering and Industrial Chemistry, University of New South Wales, Sydney, NSW 2052, Australia*

[b] *Department of Chemical Engineering, University of Newcastle, Callaghan, NSW 2308, Australia*

Received 17 November 2003; received in revised form 6 March 2004; accepted 16 March 2004

Abstract

Although the catalytic steam reforming of hydrocarbon for synthesis gas production is often carried out with excess steam-to-carbon ratio (S:C > 3), on-line catalyst deactivation due to coking invariably affects reformer performance. It is therefore necessary to obtain quantitative relation on the coupling between carbon deposition and pure steam reforming activity in order to develop optimal reformer-regenerator policy. Since kinetic information on steam reforming is often collected under carbon-free conditions, the effect of coke on the rate parameters is not fully understood. This investigation addresses the procurement of both steam reforming and deactivation kinetic constants simultaneously from transient reaction data under conditions of low steam-to-carbon ratio in a fluidised bed reactor fed with propane and employing an alumina-supported Co-Ni catalyst. Two-way ANOVA statistical treatment confirmed strong interaction between temperature and S:C ratio on the coking dynamics. Although the steam reforming kinetic constant exhibited Arrhenius dependency on temperature, the deactivation rate coefficient is characterised by a negative activation energy since carbon deposition increased with decreasing temperature in the range examined (773–873 K). This was corroborated by total organic carbon (TOC) analysis, XRD data and temperature-programmed oxidation (TPO) results of the used catalysts. The TPO spectra evidenced the formation of two types of carbonaceous pools with different C:H ratios of 1 and 6—an indication that coke formation proceeded via dehydropolymerisation of surface CH_x species to naphthalenic compounds.

Keywords: Deactivation; Coke formation; Kinetics; Propane steam reforming; Fluidised bed reactor; Cobalt-nickel catalyst; Coke characterisation; TOC; Thermogravimetry

1. Introduction

The production of high value-added petrochemicals is dependent on availability of H_2 and CO (synthesis gas mixture). Steam reforming of light alkanes is the most economical route for the manufacture of synthesis gas (H_2/CO mixture) and typically constitutes about 60% of the overall cost of the petrochemical production facility, for example, methanol and the Fischer–Tropsch process for higher hydrocarbons synthesis [1,2]. Consequently, even modest improvements in the steam reforming operation translate to substantial gains in plant economics. However, steam reforming is accompanied by significant carbon deposition via hydrocarbon dehydrogenation and/or CO disproportionation. Carbon lay-down on the catalyst surface leads to loss of active sites for the reactant (hydrocarbon and steam) adsorption [3,4]. Significantly, since the reactant (or CO product) is a deactivation-inducing agent, the traditional decoupling of reaction and deactivation kinetics suitable in other reactions is not easily accomplished for the hydrocarbon steam reforming system. For this reason, considerable efforts have gone to the development of expensive new catalyst formulations that are carbon-resilient or even novel reactor operations to minimise coking [5–7]. These have yet to find commercial applicability. Regardless, the global reaction rate for steam reforming is always influenced by the coking process and hence, kinetic parameters obtained under laboratory conditions with high steam-to-carbon ratios (S:C > 3) would be unrealistic for industrial reformer design. However, a recent method proposed by Levenspiel [8] may be used to simultaneously obtain both reaction kinetic constant and deactivation rate coefficient from on-line reactor conversion-time profile. Since the resulting

* Corresponding author. Tel.: +61-2-9385-5268; fax: +61-2-9385-5966.
E-mail address: a.adesina@unsw.edu.au (A.A. Adesina).

1385-8947/$ – see front matter © 2004 Elsevier B.V. All rights reserved.
doi:10.1016/j.cej.2004.03.005

Nomenclature

a	activity
a_s	residual activity
C_A	concentration of propane (mol L^{-1})
C_{A_0}	initial concentration of propane (mol L^{-1})
C_W	concentration of steam (mol L^{-1})
d	deactivation order
E_{A_d}	steam reforming activation energy (kJ mol^{-1})
$-E_{A_d}$	deactivation activation energy (kJ mol^{-1})
ΔG	Gibbs free energy change (kJ mol^{-1})
k	intrinsic reaction rate constant (mol s^{-1} g cat^{-1} (L $mol^{-1})^{n+m}$)
k'	steam reforming kinetic constant (mol$^{1-m_1}$ L^{m_1} s^{-1} g cat^{-1})
k_0	frequency factor (mol$^{1-m_1}$ L^{m_1} s^{-1} g cat^{-1})
$k_0{}'$	as defined in Eq. (21b) (mol$^{1-m_1}$ L^{m_1} s^{-1} g cat^{-1})
k_d	intrinsic deactivation rate coefficient (s^{-1})
$k_d{}'$	deactivation rate coefficient in Eq. (9a) (s^{-1})
$k_d{}''$	deactivation rate coefficient in Eq. (14b) (s^{-1})
k_{d_r}	intrinsic deactivation constant (mol$^{-\varepsilon_1}$ L$^{\varepsilon_1}$ s^{-1})
k_{d_0}	frequency factor for deactivation (s^{-1})
k_{d_1}	as defined in Eq. (20b) (s^{-1})
k_s	intrinsic residual deactivation constant (mol$^{-\gamma_1}$ L$^{\gamma_1}$ s^{-1})
m, n, p, q	reaction orders
R	correlation coefficient
R_g	ideal gas constant (kJ mol^{-1} K^{-1})
$-r_{SR}$	steam reforming reaction rate (mol s^{-1} g cat^{-1})
T	temperature (K)
t	reaction run time (s)
X	propane conversion
$y_{i/j}$	product ratio of i to j

Greek letters

α_C	S:C ratio
α_T	dimensionless temperature
$\delta, \varepsilon, \phi, \gamma$	reaction orders
η	C:H ratio in the coke structure
τ'	gas residence time (g cat s L^{-1})

estimates are more representative of the overall kinetics under carbon-induced catalyst decay, they may be used for further reactor optimisation. A further objective of this study was to investigate the dependency of the reaction and deactivation constants on process variables and also probe the characteristics of the coked catalysts by thermal analysis. The present study was carried out in a fluidised bed system using propane as the hydrocarbon substrate since carbon deposition and by implication, deactivation can be carried out at relatively low temperatures to minimise contribution from sintering.

Table 1
Thermodynamic characteristics of propane steam reforming and related reactions

Reaction	$\Delta G(T)$
$C_3H_8 + 3H_2O = 3CO + 7H_2$	$\Delta G_{SR}(T) = 506{,}240 - 705T$
$C_3H_8 = CH_4 + 2C\,(s) + 2H_2$	$\Delta G_{DHY}(T) = 20{,}358 - 155T$
$2CO = C + CO_2$	$\Delta G_{BOU}(T) = -167{,}424 + 164T$
$CO + H_2O = CO_2 + H_2$	$\Delta G_{WGS}(T) = -40{,}894 + 45T$

The steam reforming of propane is given by

$$C_3H_8 + 3H_2O = 3CO + 7H_2 \quad (1)$$

while carbon deposition may occur via propane dehydrogenation

$$C_3H_8 = CH_4 + 2C\,(s) + 2H_2 \quad (2)$$

or CO disproportionation (Boudouard reaction)

$$2CO = C + CO_2 \quad (3)$$

with possible water gas shift reaction (WGS)

$$CO + H_2O = CO_2 + H_2 \quad (4)$$

The thermodynamic attributes of these reactions are summarised in Table 1.

2. Experimental details

2.1. Catalyst

A catalyst with composition (by weight) 5Co:15Ni:80γ-Al_2O_3 was used. Commercial γ-alumina (Norton, USA) was pre-treated for 6 h at 1073 K to immunise it against thermally-induced phase changes in subsequent operations. The treated alumina was then sequentially impregnated with aqueous solutions of $Co(NO_3)_2$, dried and followed by re-soaking in $Ni(NO_3)_2$ solution. The addition of each nitrate was followed by 3 h of stirring at 303 K and a pH of 2 with subsequent overnight drying of the slurry in an oven at 393 K. The resulting product was calcined at 973 K for 5 h at a heating rate of 5 K min^{-1}. The calcined solid was then crushed and sieved to 212–250 μm.

2.2. Deactivation experiments

Three steam-to-carbon ratios in range of 0.8–1.6 and three reaction temperatures between 773 and 873 K were employed for the deactivation experiments. Fig. 1 is a schematic

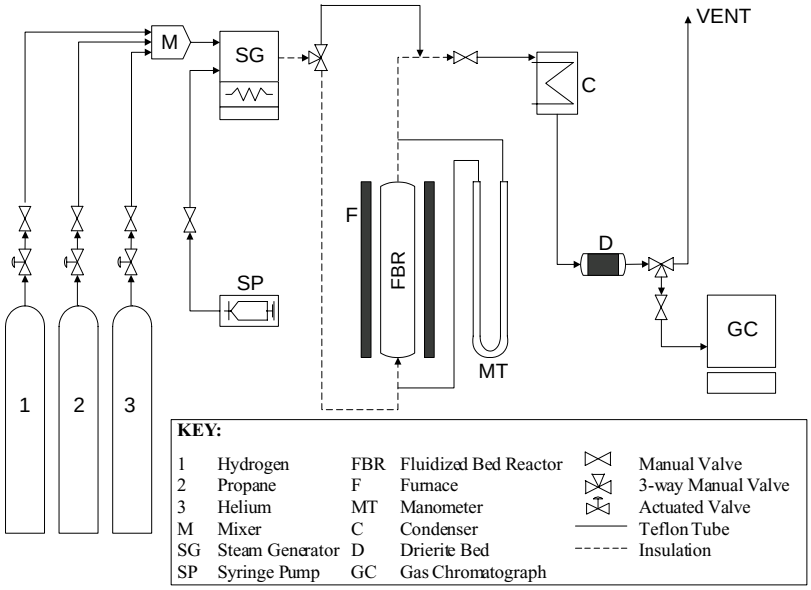

Fig. 1. Schematic diagram of the experimental set-up.

representation of the experimental rig. Deactivation runs were conducted using a fluidised bed reactor made from a quartz tube with 20 mm i.d. and 490 mm length placed vertically in an electrical furnace with a 3 mm o.d. stainless steel thermocouple positioned axially inside the bed to measure reaction temperature. For each run, 1 g of catalyst was loaded into the tube where it was supported by 3 mm thick sintered (50 μm holes) quartz as gas distributor. Prior to each run, the catalysts were reduced in pure hydrogen flow (200 mL min^{-1}) at 873 K for 2 h. The steam reforming reaction was carried out using propane (BOC Gases, Sydney) and diluent helium (Linde, Sydney) as feed mixture. Both gases were regulated by Brooks electronic mass flow controllers (model 5850E). The gas mixture was subsequently added to steam generated from ultra-pure water injection (by a Razel A-99 syringe pump) into a stainless steel coil immersed in the same water bath as the propane/helium mixing chamber. Thus, total gas flow to the reactor was maintained at 300 mL min^{-1} (at 300 K and 1 atm) to ensure particulate fluidisation operation. Insulated line at 533 K was installed between the steam generator and the reactor in order to avoid any steam condensation. Reactor effluent was passed through an ice-bath and over a drierite bed ($CaSO_4$) to remove moisture before product composition analysis on a Shimadzu gas chromatograph (model 8A) fitted with a thermal conductivity detector and an Alltech Haysep DB column. The GC was operated isothermally at 393 K using argon as the carrier gas. Each experiment was typically run for 10 h with GC sampling at interval of 40 min.

2.3. Catalyst characterisation

BET surface areas for both fresh and used catalysts were obtained by N_2 adsorption on Micromeritics ASAP 2000 unit. The used catalysts were first regenerated in the fluidised bed reactor using air (100 mL min^{-1}) at 673 K for 2 h before BET runs were conducted. The re-oxidation was carried out at a lower temperature than the reaction to minimise thermally-induced surface and morphological changes during exothermic regeneration. Spent carbon-containing catalysts were examined using various methods. A Shimadzu Total Organic Carbon (TOC) Analyzer 5000A coupled to a Solid Sample Module SSM-5000A was employed to determine the total carbon content. Catalyst solid phase analysis was obtained from the X-ray diffractograms. A Philips X'pert system using a Ni-filtered Cu Kα radiation (λ = 1.542 Å) at 40 kV and 30 mA was used for the XRD measurements. Temperature-programmed (oxidation (TPO) and reduction (TPR)) experiments to study the weight change transients were performed in a ThermoCahn TG-2121 TGA unit. TPO experiments utilised air at 55 mL min^{-1} with ramping at 5 K min^{-1} to 923 K, where the temperature was held constant for 5 h, before cooling down to room temperature in air at the same rate. TPR runs were conducted with 50% H_2/N_2 mixture at 55 mL min^{-1} using the same temperature-programming scheme as the TPO.

3. Results and discussion

3.1. Deactivation experiments

Catalyst performance was examined under conditions that deliberately favoured coking in order to assess the impact of carbon deposition during steam reforming. Fig. 2 shows typical propane conversion-time profiles as a function of steam-to-carbon ratio and temperature. The corresponding equilibrium conversions, shown as horizontal lines, are well

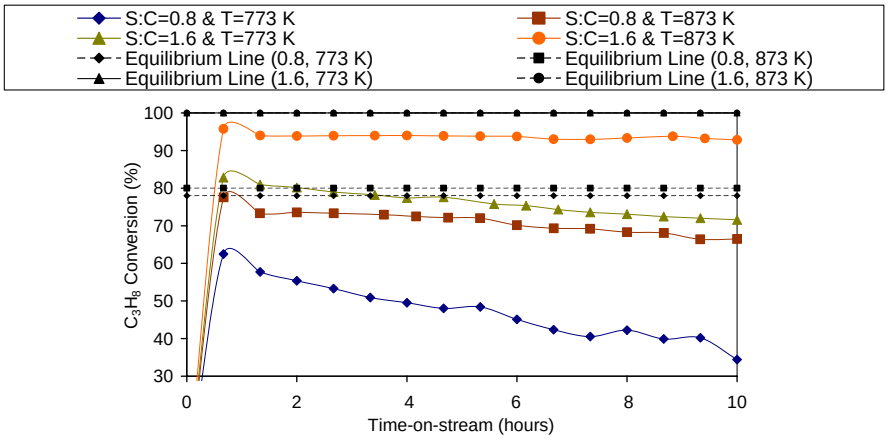

Fig. 2. Transient propane conversion profiles.

above the experimental values for all runs. The associated product selectivity curves are displayed in Fig. 3(a)–(d). H_2 and CO selectivities were generally more stable with time after about 1 h on-stream than CH_4 evincing a continuous build-up of carbon via Eq. (2). The steam reforming reaction rate, $-r_{SR}$, may be written

$$-r_{SR} = kC_W^n C_A^m a(t) \quad (5)$$

where the time-dependent catalyst activity, a, is a rate attenuation factor due to deactivation by coking and is frequently defined as the ratio of the reaction rate at any given time, $-r_{SR}(t)$, to that of the fresh catalyst, $-r_{SR}(0)$. The activity decay law,

$$-\frac{da}{dt} = k_d C_W^p C_A^q a^d \quad (6)$$

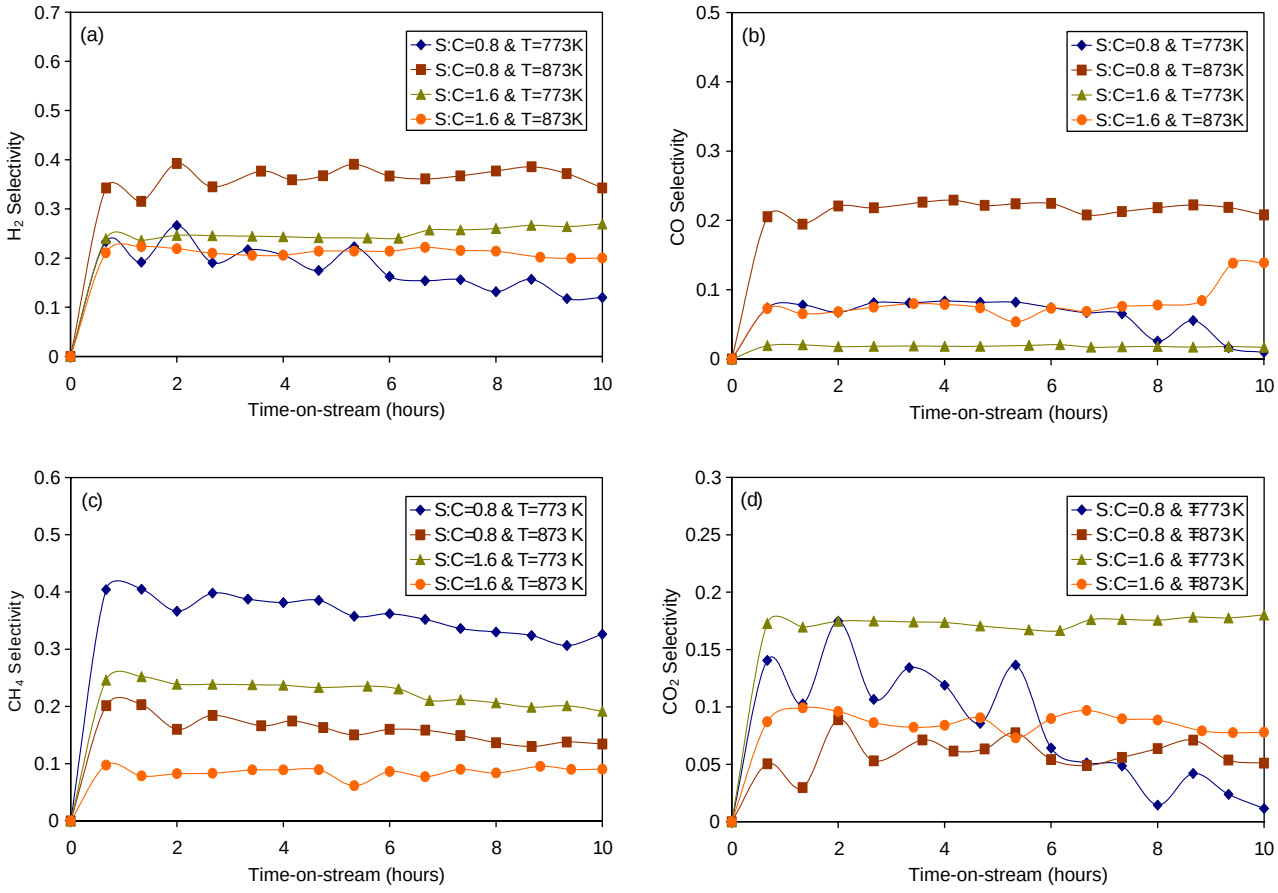

Fig. 3. Transient selectivity profiles for component: (a) H_2; (b) CO; (c) CH_4; and (d) CO_2.

which captures common deactivation models [9], viz.; linear ($d = 0$), exponential ($d = 1$) and hyperbolic ($d = 2$) provides the time-varying activity, $a(t)$. Since conversion data were collected from a well-mixed (small fluidised bed) reactor, described by

$$\tau' = \frac{X}{-r_{SR}} \tag{7}$$

using Eqs. (5) and (6) in Eq. (7) yields the expression for the concentration(conversion)-time profile in terms of kinetic and deactivation parameters [8]. Although C_W (steam concentration) and C_A (propane concentration) are independent variables, Eq. (5) may be re-expressed as:

$$-r_{SR} = k' C_A^{m_1} a \tag{8a}$$

where

$$k' = k\left(\frac{C_W}{C_A}\right)^n \quad \text{and} \quad m_1 = n + m \tag{8b}$$

Thus, k', is a pseudo-rate constant, which depends on temperature and the steam:carbon ratio, α_C (i.e. $k' = 3^{-n} k \alpha_C^n$). By same token, Eq. (6) rewrites as:

$$-\frac{da}{dt} = k'_d a^d \tag{9a}$$

where

$$k'_d = 3^{-p} k_d \alpha_C^p C_A^{q_1} \quad \text{with} \quad q_1 = p + q \tag{9b}$$

Upon integration,for $d \neq 1$

$$a = [1 + (d-1)k'_d t]^{(1/(1-d))} \tag{10}$$

while for $d = 1$,

$$a = \exp(-k'_d t) \tag{11}$$

Introducing Eqs. (8) and (10) into Eq. (7) gives,for $d \neq 1$

$$\tau' = \frac{C_{A_0} - C_A}{k' C_A^{m_1}[1 + (d-1)k'_d t]^{1/(1-d)}} \tag{12}$$

while for $d = 1$:

$$\tau' = \frac{C_{A_0} - C_A}{k' C_A^{m_1} \exp(-k'_d t)} \tag{13}$$

In principle, a fit of the C_A versus t data to either Eq. (12) or Eq. (13) should provide parameter estimates for d, k, m, n, p, q and k_d via iterative nonlinear regression analysis.

However, the highly nonlinear nature of these functions immediately shows that the Jacobian matrix of the associated function partial derivatives with respect to each of the parameters (which are themselves severely nonlinear as may be seen from Eq. (12) or Eq. (13)) is prone to singularity making nonlinear regression impracticable. Indeed, nonlinear regression with POLYMATH 5.1 failed to converge irrespective of the initial guess for the parameter estimates. In particular, from a statistical standpoint, the Gaussian error distribution in the dependent variable is unchanged for linear regression analysis, and would therefore provide more reliable parameter estimates with fewer data points. This is especially germane to the present study since it was difficult to conduct steam reforming runs with steam-to-carbon ratios, α_C, lower than 0.6 due to rapid reactor carbon blockage. Thus, linear regression analysis is the more promising option for evaluation of data from this study. The conversion-time data presented in Fig. 2 rule out the possibility of a linear ($d = 0$) or exponential ($d = 1$) deactivation model. Preliminary analysis provides correlation coefficients, R, of 0.7472 and 0.8474, respectively.

For a system with activity decay to non-zero steady-state level, the recent deactivation model proposed by Monzón et al. [10] given by

$$-\frac{da}{dt} = k''_d (a - a_s)^d \tag{14a}$$

may be used instead of Eq. (6) for the analysis carried out between Eq. (9) and Eq. (13), where

$$k''_d = k_{d_r} C_W^\delta C_A^\varepsilon \tag{14b}$$

and, the steady-state residual activity, a_s, is

$$a_s = k_s C_W^\phi C_A^\gamma \tag{14c}$$

with k_{d_r} and k_s taking on the usual Arrhenius dependency. This exercise leads to;for $d \neq 1$

$$\tau' = \frac{C_{A_0} - C_A}{k' C_A^{m_1}[a_s + \{(1 - a_s)^{1-d} + (d-1)k''_d t\}^{1/(1-d)}]} \tag{15}$$

where

$$k''_d = 3^{-\delta} k_{d_r} \alpha_C^\delta C_A^{\varepsilon_1} \quad \text{and} \quad \varepsilon_1 = \delta + \varepsilon \tag{16a}$$

$$a_s = 3^{-\phi} k_s \alpha_C^\phi C_A^{\gamma_1} \quad \text{and} \quad \gamma_1 = \phi + \gamma \tag{16b}$$

for $d = 1$:

$$\tau' = \frac{C_{A_0} - C_A}{k' C_A^{m_1}[a_s + (1 - a_s)\exp(-k''_d t)]} \tag{17}$$

It is apparent that Eqs. (15) and (17) lead to even greater number (9) of kinetic and deactivation parameters than those from Eqs. (12) to (13), thus requiring a more computationally-intensive nonlinear regression fit attended by similar statistical constraints and a larger number of data points than obtained in this study.

Although over a sufficiently long period a coked catalyst would ultimately attain a non-zero residual activity, an initial fit of the activity data in this study (for example, Fig. 2) to a hyperbolic model ($d = 2$) at constant steam:carbon ratio gave reasonable agreement (correlation coefficient: 0.9759) suggesting that Eq. (12) may be used. Consequently, for $d = 2$, we receive

$$\tau' = \frac{C_{A_0} - C_A}{k' C_A^{m_1}[1 + k'_d t]^{-1}} \tag{18}$$

whereupon linearization yields:

$$\frac{1}{(C_{A_0}/C_A) - 1} = \frac{1}{k'\tau'} + \left(\frac{k'_d}{k'\tau'}\right) t \tag{19}$$

Table 2
Parameter estimates and corresponding statistics

S:C ratio	Temperature		
	773 K	823 K	873 K
0.8			
$k' \times 10^3$	5.277 ± 0.587	7.648 ± 0.590	10.556 ± 0.370
k_d'	0.205 ± 0.041	0.164 ± 0.025	0.091 ± 0.009
R	0.950	0.962	0.975
1.2			
$k' \times 10^3$	7.455 ± 0.807	7.680 ± 0.409	12.554 ± 0.359
k_d'	0.189 ± 0.028	0.081 ± 0.013	0.032 ± 0.006
R	0.946	0.930	0.883
1.6			
$k' \times 10^3$	7.377 ± 0.474	12.047 ± 0.529	16.698 ± 1.149
k_d'	0.114 ± 0.018	0.064 ± 0.010	0.017 ± 0.008
R	0.947	0.926	0.871

The implicit assumption that $m_1 = 1$ and $q_1 = 0$ is necessary to keep the mathematics tractable but inconsequential to the parameter estimates since for other values of these exponents, the effect can be lumped into the reaction rate parameters and will therefore be reflected in the dependency of k' and k_d' on the steam:carbon ratio.

A fit of the concentration history data to Eq. (19) provided k' and k_d' estimates for various runs. Table 2 summarises these kinetic estimates and the relevant statistics. The results, show that deactivation was minimal under high S:C ratio and temperature while the steam reforming reaction was least favoured at low S:C ratio and low temperature (0.8 and 773 K, respectively). These latter conditions correspond to those for which the deactivation rate coefficient, k_d', was highest. It would therefore seem that carbon lay-down was stimulated at low S:C ratio and low temperature. Indeed, solid carbon content analysis (from TOC Solid Sample Analyser), TPO of coked specimens and XRD data (later discussed) lend credence to these findings. Carbon deposition over transition metals has been extensively studied in different laboratories [11–15]. Bartholomew [11,12] presented a study on carbon deposition rate on Ni between 673 and 1073 K. From 673 to 773 K, rate increased with temperature as expected, however, from 773 to 873 K, he observed that rate dropped to a minimum before exhibiting another Arrhenius-type behaviour up to about 1073 K. Incidentally, data in this study obtained in the range 773–873 K agreed with this inverse dependency of carbon deposition rate on temperature.

Although it would seem that the high k_d' value at low S:C ratio was due to propane dehydrogenation on a surface starved with H_2O, the drop in its value with increased S:C ratio suggests that propane reforming has become increasingly dominant. As may be seen from Fig. 4(a), k_d' value also decreased with temperature at all S:C ratios implicating a negative activation energy for the deactivation process in the temperature range studied. Indeed, from Eq. (9b)

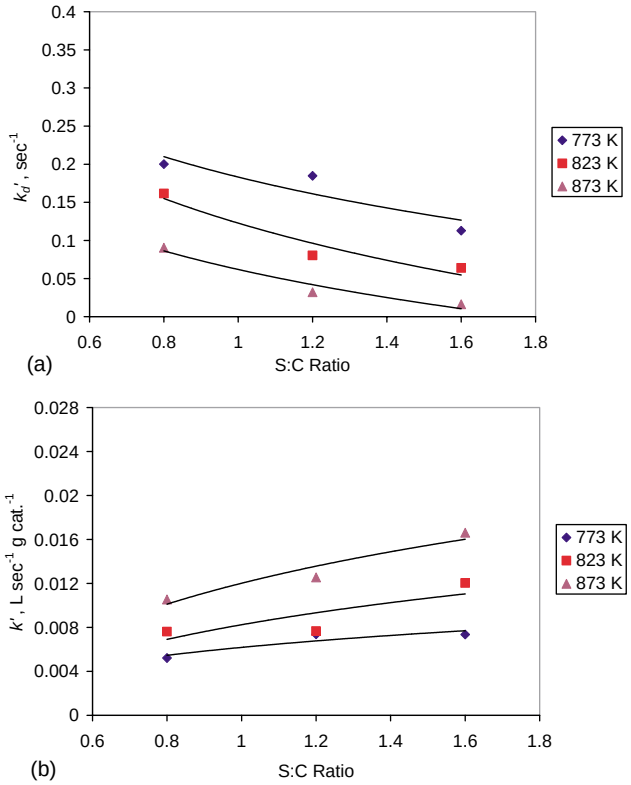

Fig. 4. Profiles of: (a) deactivation coefficient, k_d' and (b) reaction constant, k'.

$$\ln k_d' = \ln(k_{d_1}) - \frac{E_{A_d}}{R_g}\frac{1}{T} + p \ln \alpha_C \tag{20a}$$

with

$$k_d = k_{d_0} \exp(-E_{A_d}/R_g T) \quad \text{and} \quad k_{d_1} = 3^{-p} k_{d_0} \tag{20b}$$

Multilinear regression analysis of the data in Fig. 4(a) gave $p = -1.54$, $E_{A_d} = -83.7\,\text{kJ mol}^{-1}$ and $k_{d_0} = 9.35 \times 10^{-8}\,\text{s}^{-1}$ with a correlation coefficient of 0.9815. Interestingly, the $-E_{A_d}$ estimate falls within the range of activation energy for carbon formation on metal catalysts [12]. Additionally, a negative order with respect to steam ($p = -1.54$) shows that deactivation is inhibited in a steam-rich environment while the strong positive dependency on propane concentration is in agreement with coking as cause for catalyst deactivation.

On the other hand, Fig. 4(b) shows that the steam reforming rate constant, k', increased with S:C ratio and also exhibits the expected Arrhenius dependency. The corresponding expression for multilinear regression analysis being (cf. Eq. (8));

$$\ln k' = \ln(k_0') - \frac{E_A}{R_g}\frac{1}{T} + n \ln \alpha_C \tag{21a}$$

where

$$k = k_0' \exp\left(-\frac{E_A}{R_g T}\right) \quad \text{and} \quad k_0' = 3^{-n} k_0 \tag{21b}$$

Parameter estimation using data in Fig. 4(b) provides $n = 0.6$, $E_A = 38.25\,kJ\,mol^{-1}$, $k_0 = 4.39\,L\,s^{-1}\,g\,cat^{-1}$ and a correlation coefficient of 0.9698.

From the foregoing analysis, it is evident that the emergence of a negative activation energy for the deactivation reaction is not a physical oddity since the same database provided other parameters that are readily admissible. Apart from this internal consistency, the observation of a decreasing deactivation rate with increase in temperature is also mechanistically-compatible with a process in which carbon lay-down dropped with temperature since carbon deposition is the main cause for deactivation.

The nonlinear interaction between temperature and S:C ratio in the determination of hydrocarbon steam reforming kinetics has been qualitatively deduced by Bartholomew [11,12] and Yamazaki et al. [16], although complementary quantitative corroboration is unavailable. Statistically, interaction between two independent variables in a response surface analysis is symptomatic of a change in the physical or chemical mechanism underlying the process at different factor levels and may be probed by carrying out a two-way ANOVA treatment on the replicated response variable measurements. This was done for both k' and k_d' at all levels of S:C ratio and temperature used in this investigation. Table 3—which displays the calculated F-values—clearly shows that not only did temperature and S:C ratio constitute important determinants of the kinetic parameters, the S:C-temperature interaction is also statistically significant at 95% confidence level since the computed F-values were greater than the values from standard statistical tables [17].

Time-averaged product distribution during the steam reforming under low S:C ratio is also a useful indicator of the reaction complexity. Fig. 5(a) and (b) illustrate the 3D representation for the H_2:CO ratio and H_2:CO_2 ratio as a function of the two experimental variables. While the H_2:CO ratio is a signal to the 'competitiveness' of the steam reforming reaction among the four concurrent reactions, the H_2:CO_2 ratio measures the extent of the contribution by the water gas shift reaction. It is apparent that propane reforming is favoured at high S:C ratio at the low end of the temperature range used. Thus, H_2:CO ratios well in excess of stoichiometric prediction suggest that CO was either being simultaneously consumed in a companion reaction or H_2 was being formed via another route. Thermodynamics indicate that both water gas shift and Boudouard reactions—CO consuming pathways—are favoured at low temperature (as seen from Table 1) and hence, the high H_2:CO ratio observed. This is consistent with the low H_2:CO_2 ratio (high CO_2 in the product) corresponding to the region of high H_2:CO in Fig. 5(a). Under conditions of high temperature and low S:C ratio where propane dehydrogenation is preferred, a high H_2:CO_2 is observed (cf. Fig. 5(b)). The correspondingly low H_2:CO is simply an indication of limited usage of CO in the low-temperature favoured Boudouard reaction. Indeed, as may be seen in Fig. 5(c), the product stream contained relatively high CO:CO_2 ratios. Fig. 5(d) also indicates that CH_4 production was comparatively high in the region for high H_2 generation. However, the high H_2:CH_4 ratio at high temperature end would suggest that propane dehydrogenation yielded mostly H_2 and surface CH_x groups rather than desorbed CH_4. Fig. 6(a) and (b) are indicative 3D plots of the H_2 and CO yields. It is obvious that an optimum at moderate S:C ratio (ca. 1.2) and mild operating temperature (ca. 823 K) in the H_2 response surface implicates possible reincorporation of H_2 into surface carbon (to form unsaturated CH_x species) under low S:C and low temperature which may polymerise to form site-blocking carbonaceous layer responsible for high k_d' under these conditions. Even so, the H_2 per mole C_3H_8 consumed is quite close to stoichiometric value (2.33). Fig. 6(b) also confirms that CO was substantially reused within the reaction network upon primary production via steam reforming since the CO production per mole C_3H_8 consumed was lower than the value of 3 stipulated by Eq. (1). Fig. 6(c) and (d) are surface response plots for the CH_4 generated per mole C_3H_8 reacted and CO_2 produced per mole C_3H_8 consumed, respectively. Evidently, C_3H_8 conversion to CH_4 and CO were only favoured at the low temperature and high S:C ratio possibly due to steam gasification of the surface carbon by H_2 or H_2O to CH_4 and CO, respectively.

Table 4 summarises the product distribution and clearly attests the bilinear correlation to the two operating variables

Table 3
Calculated F-values from two-way ANOVA with error variance as denominator for hyperbolic decay law

	Calculated F-values[a]	
	k_d'	k'
Temperature	232.63 (2,9)	189.09 (2,9)
S:C Ratio	122.53 (2,9)	78.31 (2,9)
Temperature–S:C interaction	8.28 (4,9)	10.84 (4,9)

$F_{2,9} = 4.26$ at 95% confidence, $F_{4,9} = 3.63$ at 95% confidence. Source: Box et al. [17]. The numbers in brackets are the degrees of freedom for numerator and denominator, respectively.

[a] Calculated $F = \dfrac{\text{effect or factor variance}}{\text{error variance}}$.

Table 4
Time-averaged concentration ratios of H_2/CO, H_2/CO_2, H_2/CH_4 and CO/CO_2

S:C ratio	Temperature (K)	H_2/CO	H_2/CO_2	H_2/CH_4	CO/CO_2
0.8	773	8.72	7.88	1.15	0.92
0.8	823	4.30	10.65	2.91	2.49
0.8	873	3.92	14.93	5.41	3.82
1.2	773	15.69	3.47	2.19	0.23
1.2	823	7.07	5.43	3.29	0.81
1.2	873	5.42	11.94	5.71	3.19
1.6	773	31.73	3.56	2.63	0.11
1.6	823	11.23	4.15	3.36	0.37
1.6	873	6.45	5.72	5.83	0.96

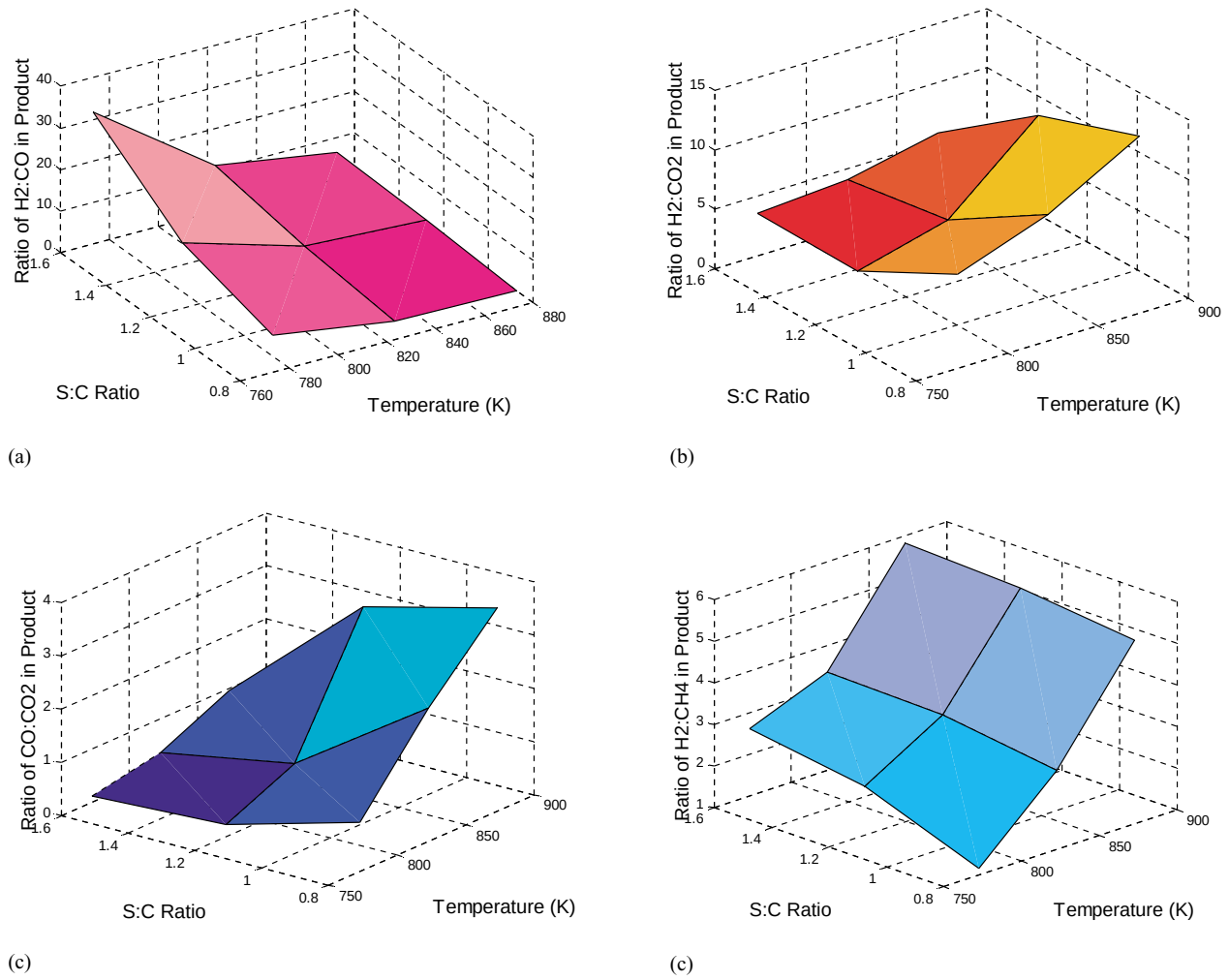

Fig. 5. Surface plots of time-averaged product ratios: (a) H_2:CO; (b) H_2:CO_2; (c) CO:CO_2; and (d) H_2:CH_4.

as described by Eqs. (22)–(25), viz.:

$$y_{H_2/CO} = 15.18\alpha_C - 0.03\alpha_T - 12.22\alpha_T\alpha_C \quad (22)$$

$$y_{H_2/CO_2} = 3.19\alpha_C + 26.34\alpha_T - 16.29\alpha_T\alpha_C \quad (23)$$

$$y_{H_2/CH_4} = 1.49\alpha_C + 5.02\alpha_T - 1.14\alpha_T\alpha_C \quad (24)$$

$$y_{CO/CO_2} = 0.17\alpha_C + 7.32\alpha_T - 4.12\alpha_T\alpha_C \quad (25)$$

where $y_{i/j}$ is the product ratio of i to j and

$$\alpha_C = \text{S : C ratio}$$

$$\alpha_T = \frac{T - 773}{100}$$

Although the data obtained may be satisfactorily explained in terms of a coke-induced deactivation, the possibility of sintering as a parallel deactivation mechanism was considered but found to be inconsistent with catalyst characterisation results. Table 5 provides the BET surface areas of freshly-calcined, freshly-reduced and oxidatively-regenerated coked specimens. Whilst there was a relatively small loss in surface area between the freshly-reduced and oxidised spent catalysts (5–16%), the latter specimens have higher surface areas than the freshly-calcined catalyst. This implies that alumina support phase changes rather than sintering was responsible for surface area variation. As discussed later, X-ray diffractogram revealed that freshly-calcined catalyst has a higher concentration of metal aluminate phase (with lower surface area) than the re-oxidised spent catalyst. In fact, the

Table 5
BET surface area of the freshly-reduced and the regenerated catalysts

S:C ratio	Temperature (K)	BET ($m^2\,g^{-1}$)
0.8	773	132.29
0.8	873	123.43
1.6	773	141.58
1.6	873	140.54
Freshly-calcined at 973 K		118.12
Freshly-reduced at 873 K		147.45

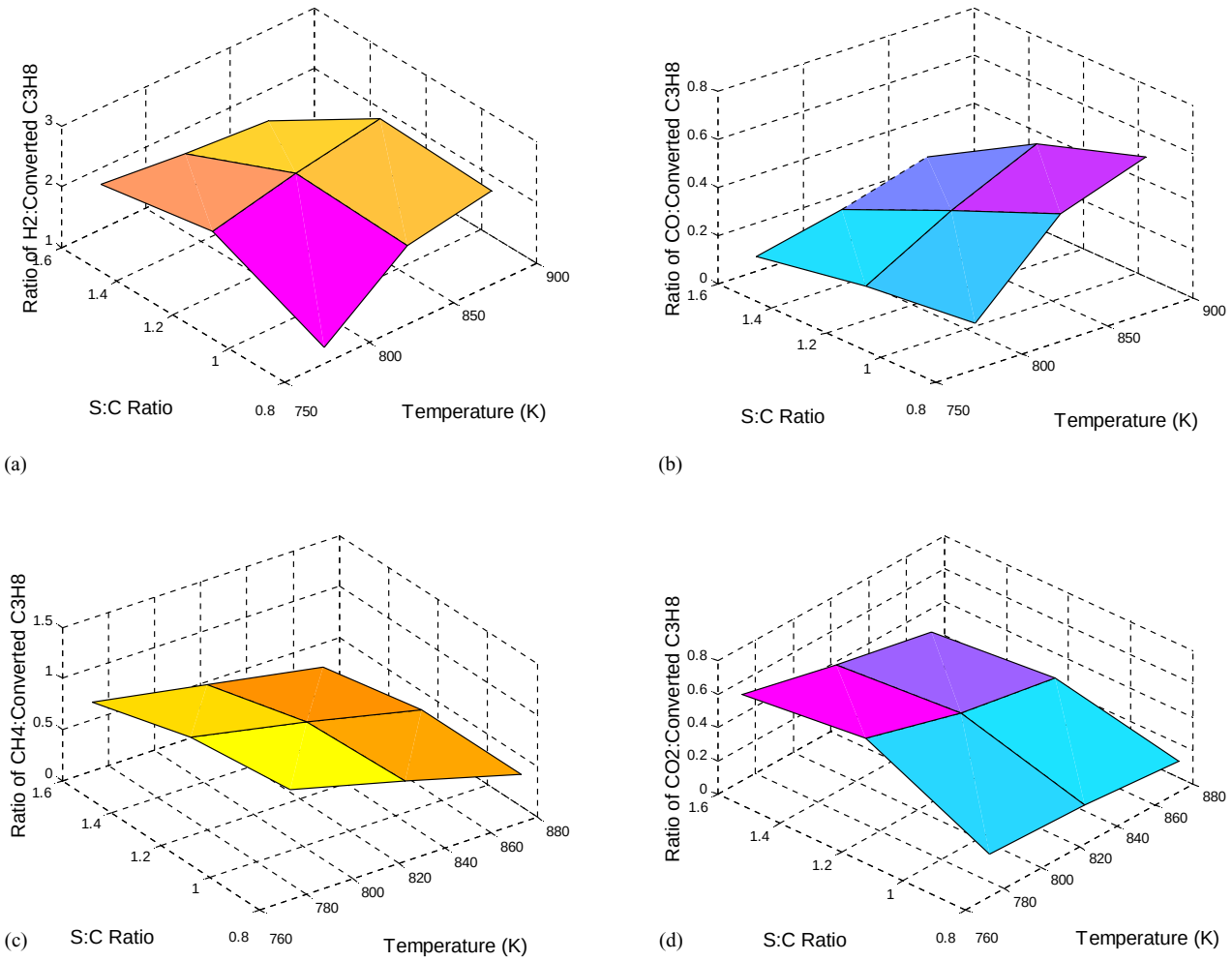

Fig. 6. Surface plots of time-averaged ratios per mole C_3H_8 consumed for component: (a) H_2; (b) CO; (c) CH_4; and (d) CO_2.

freshly-reduced catalyst with the lowest concentration of metal aluminate has the highest surface area since the metal aluminate to metal + alumina solid phase reversible reaction will proceed to different extents depending on the reducing power of the environment. Furthermore, the XRD data suggest that sintering was negligible since the metal particle size was essentially the same for catalysts with different thermal histories (cf. Fig. 8).

3.2. Carbon deposition analysis

The nature of carbon deposits formed during hydrocarbon steam reforming has been the subject of polemics [11–16]. While graphitic and amorphous carbons have been identified, Rostrup-Nielsen [18] has proposed the possibility of up to five types of carbon—vermicular, adsorbed atomic, amorphous, crystalline graphitic and bulk metal carbide. It is, nevertheless, generally conceded that the carbon-induced deactivation is caused primarily by polymeric carbon-containing moieties on the catalyst surface. The reactivity of these carbonaceous layers may be probed by temperature-programmed oxidation (or reduction). We have assigned the empirical formula $C_{1-z}H_z$ to the surface carbonaceous layer to accommodate both pure adsorbed atomic carbon ($z = 0$) and hydrogen adatoms ($z = 1$) in the composition spectrum.

Fig. 7(a)–(d) illustrate the TPO spectra of the representative coked specimens. The severely-coked samples obtained from runs with S:C = 0.8 showed substantial weight drops of 61.04% (773 K) and 57.37% (873 K). The percentage weight derivative plots for these specimens are characterized by a narrow peak and a shoulder, pointing to the presence of two types of carbonaceous compounds. Using Bartholomew's [12] nomenclature, the first peak at around 700 K may be regarded as a C_α carbon species while the polymeric C_β layer corresponds to the peak at higher oxidation temperature of about 800 K. We believe that C_β layer was formed from the polycondensation of C_α species and an equilibrium probably exists between the two pools as proposed by Rodriguez et al. [4]. Thermal oxidation profiles for the lightly-coked sample (S:C = 1.6) shown in Fig. 7(c) and (d) were accompanied by lower percentage weight drops of 14.86% (773 K) and 2.44% (873 K). Consistent with reaction-deactivation data, we note that carbon deposition

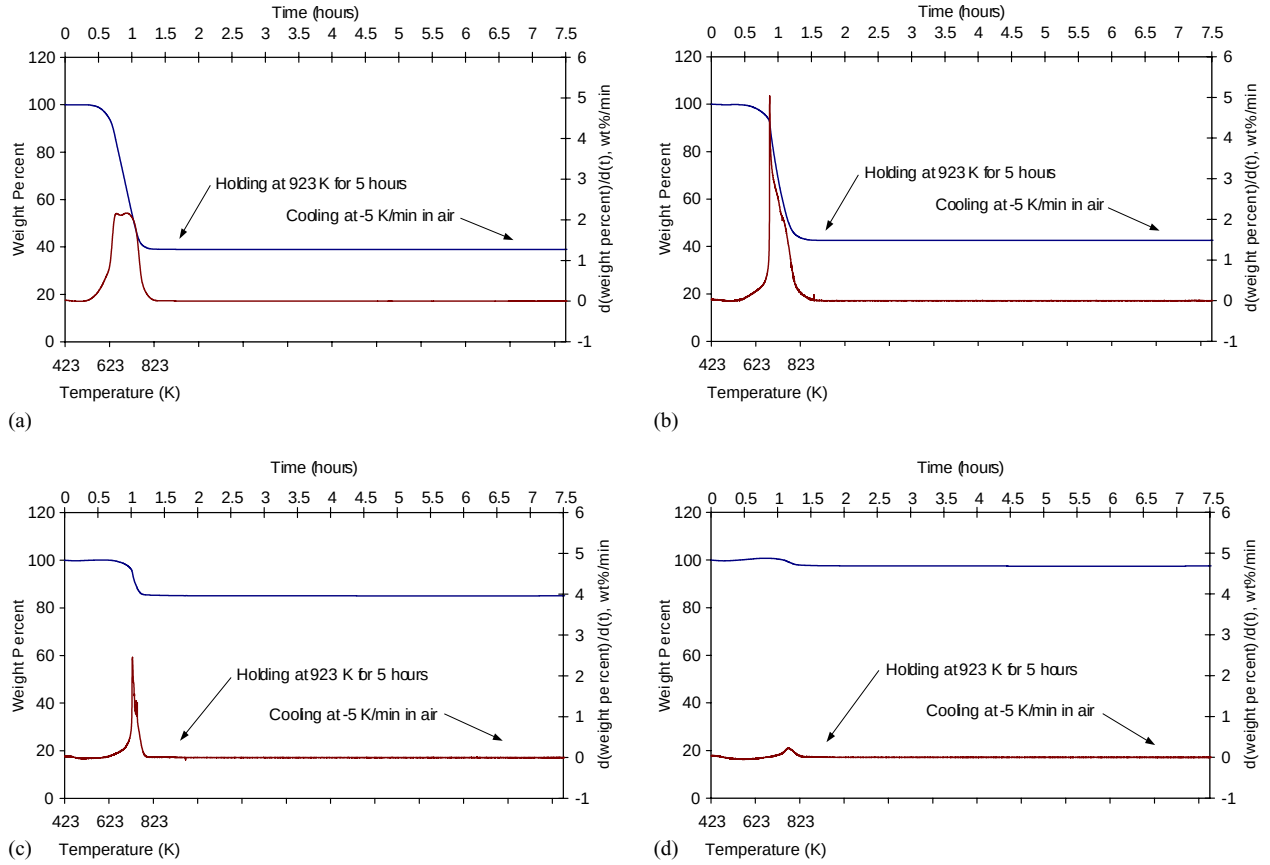

Fig. 7. TPO profiles for coked catalysts under S:C ratio and temperature of: (a) 0.8 and 773 K; (b) 0.8 and 873 K; (c) 1.6 and 773 K; and (d) 1.6 and 873 K.

was higher at lower temperature in both types of catalysts and hence the deactivation rate coefficient, k_d', would be smaller at the higher temperature resulting in the negative activation energy observed for the deactivation process. Even so, it is evident that the low temperature C_α pool was relatively small in the severely-coked samples. The weight drop (%) may be easily used to estimate the C:H ratio, η ($\eta = 1 - z/z$) for the particular carbonaceous pool. This calculation shows that for the lightly-coked specimen, z for C_α is 0.465, thus, $\eta_\alpha = 1.15$ while z for the second peak (C_β) was estimated as 0.131 giving $\eta_\beta = 6.63$. If, as initially suggested, C_β was the product of the polymerisation of C_α species, then the reaction would be accompanied by H_2 evolution in excess of stoichiometry, as was indeed the case (cf. Fig. 5(d)). Thus, the reaction may be appropriately termed a "dehydropolymerisation" step. Interestingly, studies by Fortazzi and Lietti [3] and Guisnet and Magnoux [19] indicated that coke contains primarily naphthalenic (aromatic) carbon rings consistent with C_6 structures implicated in this study.

To investigate the nature of the bulk phase, XRD measurements in Fig. 8 were collected from four used catalysts (two lightly-coked at high and low temperature; two severely-coked at high and low temperature), as well as on the calcined and freshly-reduced samples. The calcined sample contained mostly Ni and Co aluminates with modest amounts of $NiCo_2O_4$, which were easily reduced to Ni (44.5°) and Co (44.2°) phases in the freshly-reduced catalysts. The presence of $CoAl_2O_4$ (36.7°) and $NiAl_2O_4$ (37 and 44.8°) in the reduced catalyst shows that at the reduction temperature (873 K) the metal aluminates were not completely removed. Although traces of Ni and Co species may be seen in the re-oxidised coked samples, complete re-oxidation to the corresponding metal aluminate was lacking as evidenced by the lower intensities of these phases. Hence, the re-oxidised catalyst is primarily a metal oxide/Al_2O_3 system rather than a metal aluminate. Since the latter is formed at higher temperature and hence a lower surface area solid, the re-oxidised samples would have a higher BET area than the original calcined specimen consistent with BET data in Table 5. The appearance of Ni and Co crystallites in the re-oxidised coked catalyst suggests that it may be re-usable for steam reforming at comparable level of activity as in the freshly-reduced catalyst since the peak intensities are almost identical in both types of catalysts. It is evident that the Ni/Co metal particle size in both freshly-reduced and coked catalysts, are practically the same—an indication that metal sintering did not occur to any appreciable extent and therefore least likely to be a cause of catalyst deactivation. The carbon peaks (26°) observed in the coked catalysts revealed that carbon content was greater at 773 K than at 873 K while increased S:C ratio gave reduced peak intensity in agreement with the trend

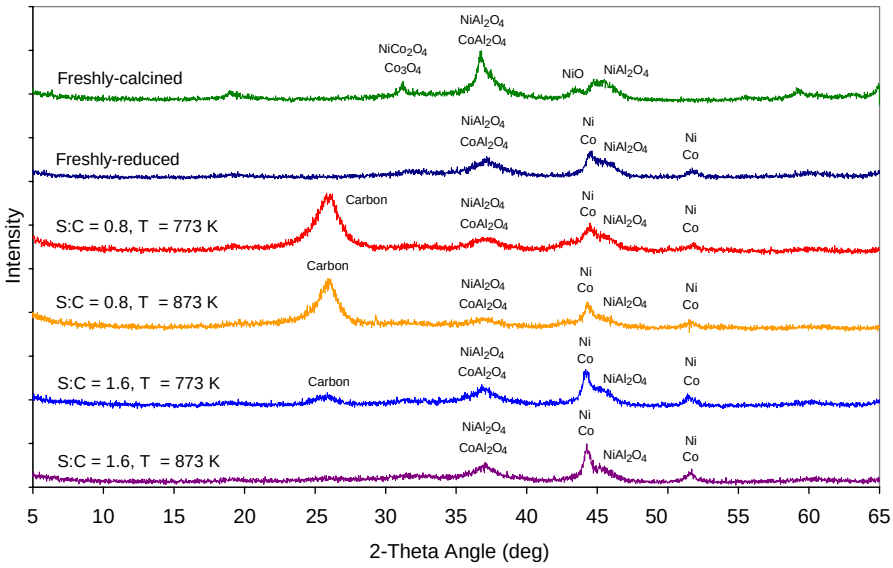

Fig. 8. X-ray diffractograms of freshly-calcined, freshly-reduced and coked catalysts.

from total organic carbon analysis displayed on Table 6. It is clear from this table that carbon content decreased with increasing temperature and S:C ratio.

Hydrogen temperature-programmed reduction data obtained immediately after TPO are shown in Fig. 9(a)–(d). All oxidized used catalysts exhibited almost identical weight drops, viz.; 5.16, 5.26, 5.19 and 5.10% after reduction. This confirms that the carbonaceous deposits were completely oxidized to CO_2 in the previous TPO runs and the catalysts were probably re-oxidized to similar oxidation states

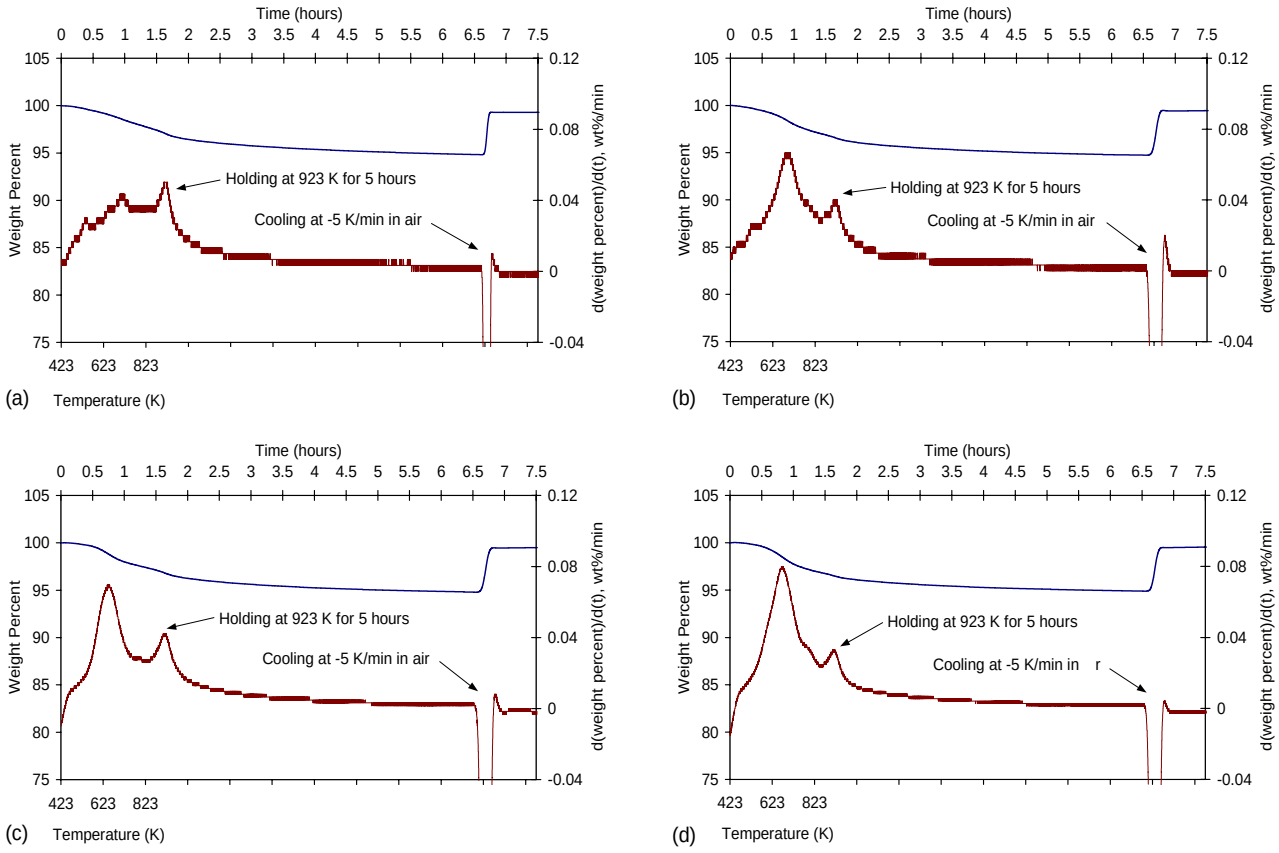

Fig. 9. TPR (following TPO in Fig. 7) profiles for coked catalysts under S:C ratio and temperature of: (a) 0.8 and 773 K; (b) 0.8 and 873 K; (c) 1.6 and 773 K; and (d) 1.6 and 873 K.

Table 6
Total carbon analysis of coked specimens

S:C ratio	Temperature (K)		
	773	823	873
0.8	60.83%	56.34%	55.15%
1.2	24.67%	9.17%	7.49%
1.6	15.09%	1.27%	0%

irrespective of the steam reforming history. The TPR spectra exhibited multiple peaks (albeit with varying heights) attributed to Ni_2O_3 (460 K), Co_3O_4 (650 K), NiO (780 K) and $NiAl_2O_4$ (920 K) and have been similarly identified by others [20–23]. The fact that $NiAl_2O_4$ could only be reduced at 920 K is in agreement with the XRD data, which showed that this phase was present in all coked and fresh specimens.

4. Conclusions

This study has examined the effect of both steam-to-carbon ratio and temperature on deactivation. Conversion-time data during steam reforming were fitted to a transient reactor-model incorporating both reaction and deactivation kinetics in a well mixed fluidised bed. Estimates of the rate constant and deactivation coefficient exhibited strong dependency on both S:C ratio and temperature. Interaction between these factors was confirmed by both qualitative and statistical (two-way ANOVA) analyses. Thermal analysis spectra (TPO–TPR) also revealed the existence of two types of carbonaceous deposits (C_α and C_β) on the catalyst. TGA empirical analysis indicates that the dehydropolymerisation of C_α to C_β species was responsible for coke formation. The C_β carbonaceous deposit appears to contain polymeric naphthalenic rings primarily responsible for deactivation.

Acknowledgements

This work was supported by an Australian Research Council grant. KMH is grateful for a University Postgraduate Award scholarship from the University of New South Wales. TTY thanks the Singapore government for a student exchange bursary. The authors are also indebted to one reviewer for constructive comments on the kinetic analysis.

References

[1] J.R. Rostrup-Nielsen, Industrial relevance of coking, Catal. Today 37 (1997) 225–232.
[2] J.R. Rostrup-Nielsen, New aspects of syngas production and use, Catal. Today 63 (2000) 159–164.
[3] P. Fortazzi, L. Lietti, Catalyst deactivation, Catal. Today 52 (1999) 165–181.
[4] J.C. Rodriguez, E. Romeo, J.L.G. Fierro, J. Santamaria, A. Monzon, Deactivation by coking and poisoning of spinel-type of Ni catalysts, Catal. Today 37 (1997) 255–265.
[5] T. Borowiecki, G. Giecko, M. Panczyk, Effects of small MoO_3 additions on the properties of nickel catalysts for the steam reforming of hydrocarbons II. Ni-Mo/Al_2O_3 catalysts in reforming, hydrogenolysis and cracking of *n*-butane, Appl. Catal. A: Gen. 230 (2002) 85–97.
[6] Y. Liu, T. Hayakawa, K. Suzuki, S. Hamakawa, T. Tsunoda, T. Ishii, M. Kumagai, Highly active copper/ceria catalysts for steam reforming of methanol, Appl. Catal. A: Gen. 223 (2002) 137–145.
[7] K. Opoku-Gyamfi, A.A. Adesina, Forced composition cycling of a novel thermally self-sustained fluidised-bed reactor for methane reforming, Chem. Eng. Sci. 54 (1999) 2575–2583.
[8] O. Levenspiel, Commentaries: chemical reaction engineering, Ind. Eng. Chem. Res. 38 (1999) 4140–4143.
[9] H.S. Fogler, Elements of Chemical Reaction Engineering, Prentice Hall, New Jersey, 1999.
[10] A. Monzón, E. Romeo, A. Borgna, Relationship between the kinetic parameters of different catalyst deactivation models, Chem. Eng. J. 94 (2003) 19–28.
[11] C.H. Bartholomew, Mechanisms of catalyst deactivation, Appl. Catal. A: Gen. 212 (2001) 17–60.
[12] C.H. Bartholomew, Carbon deposition in steam reforming and methanation, Catal. Rev. Sci-Eng. 24 (1982) 67–112.
[13] M. Larsson, M. Hulten, E.A. Blekkan, B. Andersson, The effect of reaction conditions and time on stream on the coke formed during propane dehydrogenation, J. Catal. 164 (1996) 44–53.
[14] H. Liu, L. Su, H. Wang, W. Shen, X. Bao, Y. Xu, The chemical nature of carbonaceous deposits and their role in methane dehydroaromatization on Mo/MCM-22 catalysts, Appl. Catal. A: Gen. 236 (2002) 263–280.
[15] L. Kepinski, B. Stasinska, T. Borowiecki, Carbon deposition on Ni/Al_2O_3 catalysts doped with small amounts of molybdenum, Carbon 38 (2000) 1845–1856.
[16] O. Yamazaki, K. Tomishige, K. Fujimoto, Development of highly stable nickel catalyst for methane-steam reforming reaction under low steam to carbon ratio, Appl. Catal. A: Gen. 136 (1996) 49–56.
[17] G.E.P. Box, W.G. Hunter, J.S. Hunter, Statistics for Experimenters, Wiley, New York, 1978.
[18] J.R. Rostrup-Nielsen, Catalytic steam reforming, in: J.R Anderson, M. Boudart (Eds.), Catalysis, Science and Technology, Springer-Verlag, Berlin, 1984.
[19] M. Guisnet, P. Magnoux, Organic chemistry of coke formation, Appl. Catal. A: Gen. 212 (2001) 83–96.
[20] B. Mile, D. Stirling, M.A. Zammitt, A. Lovell, M.J. Webb, TPR studies of the effects of preparation conditions on supported nickel catalysts, J. Mol. Catal. 62 (1990) 179–198.
[21] G. Jacobs, T.K. Das, Y. Zhang, J. Li, G. Racoillet, B.H. Davis, Fischer–Tropsch synthesis: support, loading, and promoter effects on the reducibility of cobalt catalysts, Appl. Catal. A: Gen. 233 (2002) 263–281.
[22] C. Li, Y.-W. Chen, Temperature-programmed-reduction studies of nickel oxide/alumina catalysts: effects of the preparation method, Thermochim. Acta 256 (1995) 457–465.
[23] H.-S. Roh, K.-W. Jun, W.-S. Dong, J.-S. Chang, S.-E. Park, Y.-I. Joe, Highly active and stable Ni/Ce-ZrO_2 catalyst for H_2 production from methane, J. Mol. Catal. A 181 (2002) 137–142.